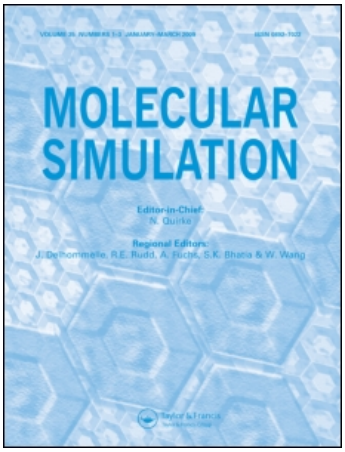

Molecular Simulation
Publication details, including instructions for authors and subscription information:
http://www.informaworld.com/smpp/title~content=t713644482

Modelling of poly(4-vinyl pyridine) and poly(4-vinyl pyridine)/pyridine composites: structural and optical properties

E. Vaganova[a]; N. Berestetsky[a]; S. Yitzchaik[a]; A. Goldberg[b]
[a] Institute of Chemistry, Hebrew University of Jerusalem, Jerusalem, Israel [b] Accelrys Inc., San-Diego, CA, USA

To cite this Article Vaganova, E. , Berestetsky, N. , Yitzchaik, S. and Goldberg, A.(2008) 'Modelling of poly(4-vinyl pyridine) and poly(4-vinyl pyridine)/pyridine composites: structural and optical properties', Molecular Simulation, 34: 10, 981 — 987
To link to this Article: DOI: 10.1080/08927020802256041
URL: http://dx.doi.org/10.1080/08927020802256041

Molecular Simulation
Vol. 34, Nos. 10–15, September–December 2008, 981–987

Taylor & Francis
Taylor & Francis Group

Modelling of poly(4-vinyl pyridine) and poly(4-vinyl pyridine)/pyridine composites: structural and optical properties

E. Vaganova[a]*, N. Berestetsky[a], S. Yitzchaik[a] and A. Goldberg[b]

[a]*Institute of Chemistry, Hebrew University of Jerusalem, Jerusalem, Israel;* [b]*Accelrys Inc., San-Diego, CA, USA*

(*Received 22 January 2008; final version received 27 May 2008*)

The interactions of the polymer poly(4-vinyl pyridine) moieties with free pyridine molecules in concentrated solution develop protonated and hydrogen-bonded species on the polymer backbone and turn the viscous solution to gel. Direct irradiation at proton transfer centre on the protonated polymer moiety promotes an amorphous-to-crystalline transition. The polymer crystals exhibit completely different optical properties when compared to the amorphous material. The proposed mechanism of the photoinduced crystallisation is the following: direct excitation to the proton transfer centre generates in abundance protonated polymer moieties, which have rigid quinone structure. Rigid quinone conformations stimulate the crystallisation of the polymer chains; in their turn, increasing polymer ordering stabilises the photoinduced protonated species. Photoinduced phase transition is reversible, meaning, that crystalline phase is metastable. To clarify the mechanism of the phase transition, in the present issue, using molecular modelling, we investigate the conformational behaviour of the polymer species depending on the state of protonation, interaction with adjacent solvent molecules and polymer side-chain units. The Density Functional Theory (DFT) calculations show the protonated pyridine moiety as a quinone structure that is clearly stable, thus emphasising the ability of such structure to play a key role as a 'working' species.

Keywords: DFT calculations; general gradient approximation; self-consistent field; pyridine; polymer; ZINDO semiempirical approximation

1. Introduction

Polymeric gels, which have been called semidilute polymer solutions by P.G. De Gennes [1], have not found wide application in the practical optical or electronic or memory storage devices, mainly due to their weak mechanical properties. However, they are nevertheless the subject of extensive investigations [2–5]. One of the main reasons for the continuing interest in polymer gels is the unique flexibility of their structural properties. The ability of polymer chains to adopt different conformations depends on the properties of the solvent and on intra or intermolecular noncovalent bonding. The driving forces for gelation include hydrogen bonding, ionic interactions, van der Waals attraction, dispersion forces and aromatic stacking. Another unique property of gels is the wide scale of external factors that can be control the structure [6–11].

The present study was stimulated by a unique material – a poly(4-vinyl pyridine)/pyridine gel [12]. When the polymers are dissolved in pyridine, the initially viscous solution spontaneously gels during storage in the dark for approximately one month. This gel is amorphous and sensitive to light. Under irradiation at 385 nm the gel transforms into a nanocrystalline material. The optical properties of the nanocrystalline material are completely different from those of the amorphous gel. Instead of blue emission at 440 nm, a set of red-shifted emission peaks appeared under irradiation at 385 nm during not less than an half an hour (light intensity 5.3 mW/cm^2) [13]. In complete agreement with the changes in the emission properties and changes in the absorption of the gel were also documented. Beginning with an irradiation time of 15 min, the gel begins to acquire a yellow colouring which deepens as the irradiation continues. The prolonged tail of the absorption in the wide wavelength range 300–400 nm grows significantly as a function of the length of the irradiation. However, the photoinduced process is reversible.

Recent spectroscopic investigation explained the sensitivity of the gel to irradiation at 385 nm. The absorption centred at 385 nm is related to a proton transfer centre on the protonated polymeric pyridine [14]. An FTIR study clarified the process of the formation of protonated centres on the polymer chain: immediately after solvation, zwitterions formed on the polymeric pyridine. In spite of the comparatively low concentration, the self-protonated polymeric pyridine species was detected by FTIR measurements as the final stage of such a charge-separated system [15].

Using molecular modelling we investigate the conformational behaviour of the pyridine polymer side-chains depending on the state of protonation, interaction with solvent and single model of a polymer unit, numbers of side-chain units on the alkane chain. In order to justify the models, we inspect the calculated UV absorption

*Corresponding author. Email: gv@cc.huji.ac.il

ISSN 0892-7022 print/ISSN 1029-0435 online

DOI: 10.1080/08927020802256041
http://www.informaworld.com

spectra of the geometry optimised model structures and compare them with the experimental spectra of absorption. To investigate the molecular reactivity of those models, we evaluate ionisation potential (IP).

2. Computation details

The computational results were obtained using software programs from Accelrys Inc. (San Diego, CA, USA) [16]. DFT calculations were performed with the DMol^3 programme [17,18], and graphical displays were generated with Materials Studio® [16]. We took advantage of the version of DMol^3 using Materials Studio 4.1 graphical interface. A double numerical polarised (DNP) basis set was employed that includes all occupied atomic orbitals plus a second set of valence atomic orbitals plus polarised d-valence orbitals. For exchange and correlation, we have applied the gradient-corrected approach using the generalised gradient approximation (GGA) functional in the manner suggested by Perdew and Wang (PW91) [19,20].

The spin-unrestricted approach was applied with all electrons being considered explicitly. In all calculations, atom-centred grids were used for numerical integration using about 2000 grid points for each atom. A real space cut-off of 7.0 Å was imposed [16,17]. The self-consistent-field (SCF) convergence criterion was set to be that the root mean square (rms) change in the electron density must be less than 1×10^{-6} electron/Å^3. Geometries were optimised using efficient algorithm taking the advantage of delocalised internal coordinates [21]. The convergence criteria applied for geometric optimisation were 1×10^{-5} Ha (Hartree units) for energy, 0.002 Ha/Å for force and 0.005 Å for displacement.

The vertical IP was obtained as the energy difference between the total energies of the cation and its neutral form with the geometry optimised for the neutral molecule. Similarly, the electron affinity (EA) was obtained as the energy difference between the total energy of the anion and the neutral molecule with the structure optimised for the anion.

The absorption spectra were calculated using the Zerner's intermediate neglect of differential overlap (ZINDO) [22] semiempirical approximation with the Intermediate Neglect of Differential Overlap (INDO)/2 Hamiltonian as implemented in the program VAMP [23] (Accelrys, Inc.). In the current calculation, 8π orbitals with 16 electrons were included into the active space of the Configuration Interactions Calculations with all single excitations (CIS) expansion. This choice allows to account for all the valence π, π*orbitals and electrons.

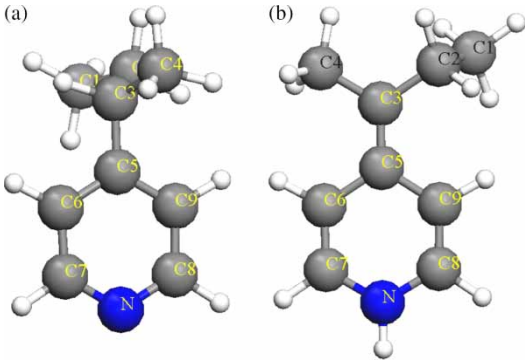

Figure 1. Model of MPP with non-protonated (a) and protonated (b) pyridine moieties.

3. Results and discussion

As mentioned above, FTIR measurements showed that the origin of the light sensitive system lies with the self-protonated side-chain unit on the backbone of poly(4-vinyl pyridine) [15]. To investigate the effect of the self-protonation on the conformational behaviour of the polymer side-chains, we modelled the molecular structure of the polymer side-chain units as 4-(1-methylpropyl) pyridine (MPP; Figure 1). Two ground state forms: non-protonated (first structure) and self-protonated (second structure), are presented in Figure 1(a) and (b), respectively. We identified the MPP in which the CH

Table 1. Bond distances; bond angles; torsional angles between alkane chain and pyridine ring; and λ_{max} of the calculated UV absorption spectra.

Parameter	1a	1b	3a	3b	6a	6b
r(C(3)—C(5)] (Å)	1.496	1.358	1.497	1.358	1.397	1.397
r(C(5)—C(9)) (Å)	1.401	1.455	1.402	1.455	1.438	1.438
r(C(9)—C(8)) (Å)	1.405	1.360	1.405	1.360	1.364	1.364
r(C(8)—N(1)) (Å)	1.348	1.387	1.348	1.387	1.418	1.418
ang(C(6)—C(5)—C(9)) (°)	118.04	114.36	118.05	114.36	115.57	115.57
ang(C(7)—N(1)—C(8))(°)	117.07	118.532	117.060	118.532	116.882	116.882
ang(N(1)—C(8)—C(9))(°)	123.645	122.03	123.595	122.03	121.428	121.428
ang(C(8)—C(9)—C(5))(°)	118.836	121.489	121.447	121.489	121.466	121.466
Torsional angle *Θ*(°)	61.7	−2.8	65.5	−0.1	−5.5	−2.8
λ_{max} (taking from the calculated UV absorption spectra; nm)	175	175, 220, 300	180	300	195, 300	195, 300

Models: MPP, 1a,b; oligomer, 3a,b; complexes, 6a,b; for non-protonated (a) and self-protonated (b) type structures.

bond on the alkane carbon C_3 is cleaved, and the 'liberated' proton are attached to the pyridine nitrogen as a model of a self-protonated pyridine polymer unit. A negative charge is concentrated on the carbon C_3 of the alkane chain, and a positive charge – on the pyridine nitrogen. The C_3–N proton transfer radically changes the molecular conformation. A comparison of the geometric parameters of the first and second structures is presented in Table 1 (columns a and b – non-protonated and self-protonated MPP, respectively). In particular:

(1) The atomic rearrangement results in a change in the calculated bond lengths. The bond lengths: *r*(C(3)—C(5)) are significantly shorter in the 'second structure' − 1.358 Å as compared to 1.496 Å in the 'first structure'; the *r*(C(6)—C(7)) bond behaves similarly. The length of the bond *r*(C(9)—C(8)) are also considerably shorter in the 'second structure' − 1.360 Å as compared to its length of the 'first structure' − 1.405 Å.

(2) A key structural parameter – the torsion angle (Θ), linking the alkane chain and the pyridine ring – significantly different in the two structures. The planar ring is bent 61.4° in the 'first structure', while the protonated pyridine unit is practically parallel to the alkane chain. In the latter case, the ring is rotated ~2.8° away from the direction of the alkane chain (Table 1, columns 1a and b, respectively).

These calculations clearly identified the self-protonated pyridine unit as a rigid resonance structure of the quinine form. The calculated UV absorption spectra of the two structures are (Figure 2(a) and (b), the 'first' and 'second structure', respectively). The UV absorption spectrum of the first model has a single peak at 195 nm; in contrast, the UV absorption spectrum of the second structure has three peaks – at 195, 220 and 300 nm. In order that the model approaches the actual polymer more closely, we expand the number of polymer units on the alkane chain and investigate the effect of side-chain self-protonation on the five-unit oligomer model. Oligomer models with non-protonated (1) and self-protonated (2) units are presented in Figure 3(a) and (b) – (1) and (2), respectively.

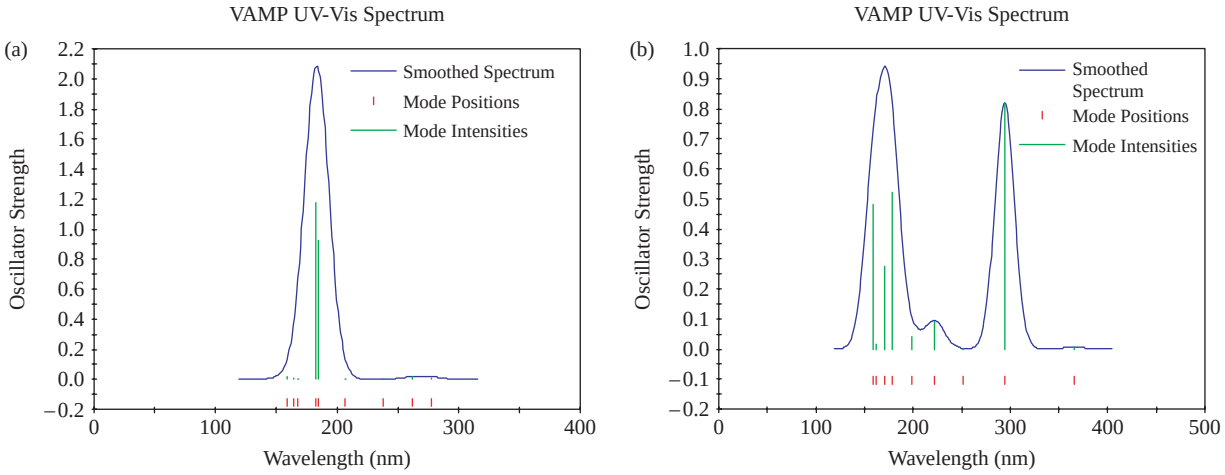

Figure 2. Calculated UV absorption spectra (VAMP) of MPP non-protonated (a) (Figure 1(a)); and protonated (b) (Figure 1(b)) pyridine moieties.

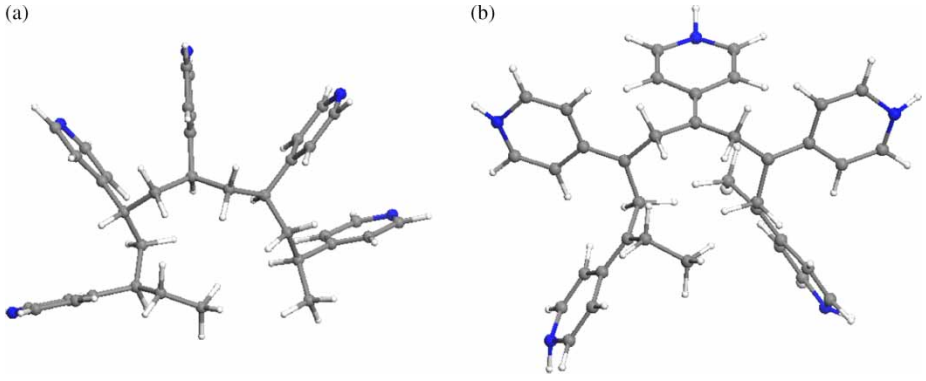

Figure 3. Models of five unit oligomers with non-protonated (a) and protonated (b) pyridine moieties.

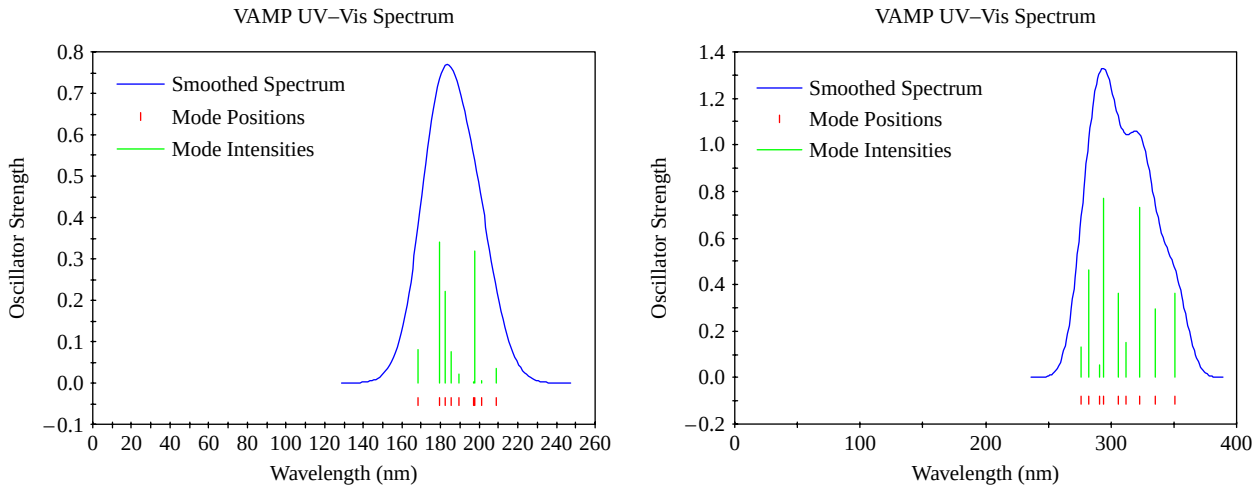

Figure 4. Calculated UV absorption spectra (VAMP) of five units oligomer of non-protonated (a) (Figure 3(a)); and protonated (b) (Figure 3(b)) pyridine moieties.

A comparison of these structures at first shows that both type of oligomers exhibit strong similarity to the isotactic structure (Figure 3). The calculated bond distances and bond angles are identical to those of the MPP models are not affected by the mutual interaction of adjacent species (Table 1, columns 3a and b, (1) and (2), respectively). The calculated values of the torsional angle (Θ) are also practically not affected by the number of moieties in the oligomer. The large difference in Θ was found only for the end-group (non-protonated) of oligomer (1) 14.5°, in contrast to the value of Θ for the other units, 69.8°–60.5°.

Although the geometric parameters are not affected by the number of the units in the oligomer, this parameter strongly influences the optical properties. The calculated UV absorption spectra reveal drastic changes in response to the increasing number of pyridine rings on the chain. In detail:

(1) oligomer (1) as well as oligomer (2) exhibit broadening of the calculated absorption spectra (Figure 4a,b), which can be the evidence of long-range electron density overlap.
(2) the molecular arrangement of the five protonated structures in oligomer (2) leads to a considerable red-shift of λ_{max}. λ_{max} is shifted to 270 nm with a pronounced shoulder at 330 nm, instead of appearing at 195 nm as in the non-protonated oligomer structures, where there is no spectral red-shift (Figure 4a,b).

We also investigated the ability of the oligomers to form a crystalline structure. The calculated crystalline structure is shown in Figure 5. The model crystal exhibits 3D monoclinic B symmetry with unit cell axes: *a*, 6.863 Å; *b*, 39.810 Å; *c*, 13.527 Å; $\alpha = \gamma$; $\beta = 93.3°$.

To determine the effect of the adjacent molecules on the conformational behaviour and optical spectra, we modelled the following complexes: MPP (self-protonated pyridine unit)/pyridine (Figure 6(a)); MPP (self-protonated pyridine unit)/MPP (non-protonated pyridine unit) (Figure 6(b)). The calculated bond distances, bond angles and torsional angles are presented in Table 1, columns 6a and 6b.

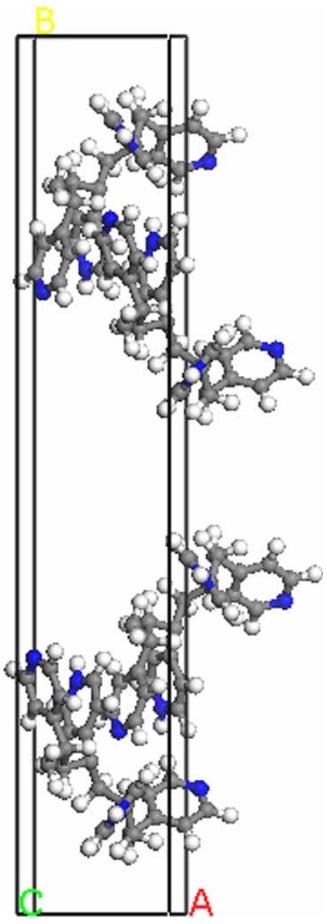

Figure 5. Model of the poly(4-vinyl pyridine) crystal structure.

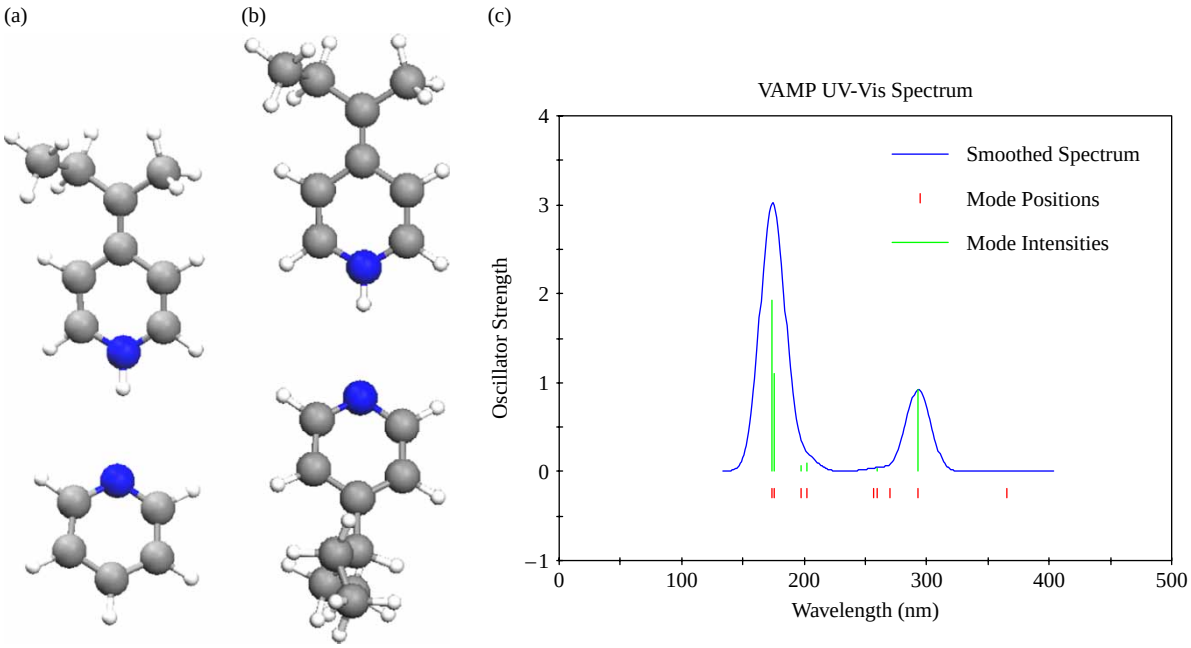

Figure 6. Models of the complexes: (a) MPP (self-protonated pyridine unit)/pyridine; (b) MPP (self-protonated)/MPP (non-protonated pyridine unit). (c) Calculated UV absorption spectra.

The geometric parameters of the self-protonated pyridine unit are identical in both complexes and have a strong similarity to the geometric parameters in the case of the isolated MPP. In addition, both structures also have identical calculated UV absorption spectra (Figure 6(c)). When compared to the single MPP, the calculated UV spectrum has the same positions of the spectrum λ_{max} however, the intensity of absorption at 300 nm is lower, compare to the former (Figure 6(c)).

To summarise the investigation of the model structures we can conclude that the self-protonation significantly affect the atomic arrangement – convert an aromatic structure to quinone conformation; rearrangement of the torsional angle lead to the alignment of the molecular species along the alkane bond, thus significantly affect the optical properties of this pyridine unit, thus affecting the energy band gap of the molecule. Increasing the number of the protonated pyridine units on the alkane chain lead to the broadening and significant red-shift of optical spectra, narrowing the molecular band gap.

To verify the model, we compared the calculated UV absorption spectra with the principal experimental absorption spectra of liquid pyridine (Figure 7); the

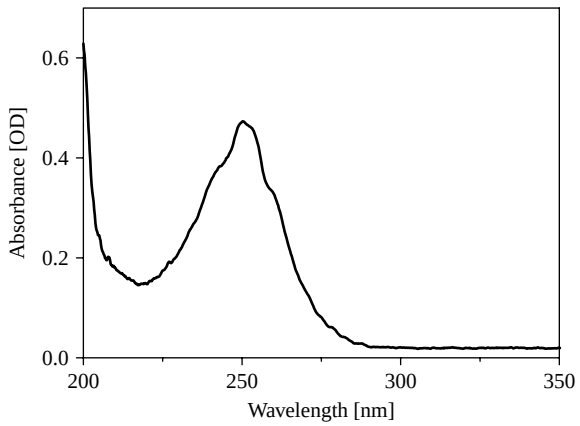

Figure 7. Room temperature absorption spectrum of a thin layer of liquid pyridine placed between two quartz slides.

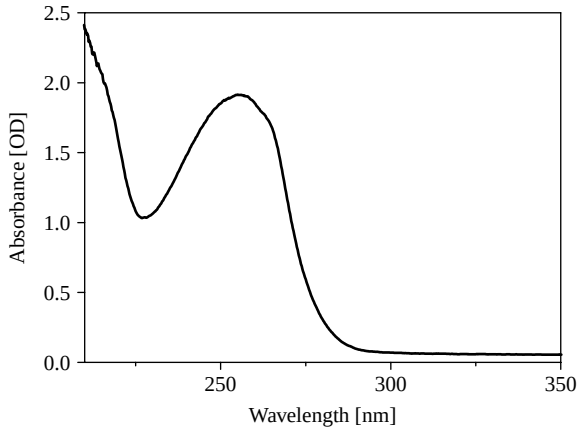

Figure 8. Room temperature absorption spectrum of a solution of the polymer P4VPy, dissolved in pyridine (one side-chain unit per one free pyridine molecule). A thin layer of the solution was placed between two quartz slides.

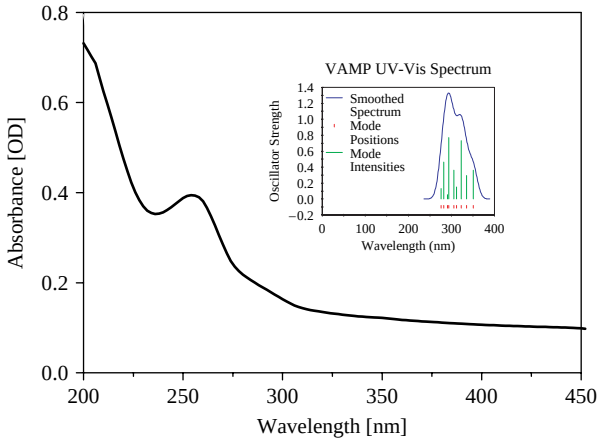

Figure 9. Room temperature absorption spectrum of the gel: polymer P4VPy, dissolved in pyridine (one side-chain unit per one free pyridine molecule) gelled spontaneously in the dark under nitrogen atmosphere during a period of 25 days. The gel was in the form of a thin film placed between two quartz slides. For comparison, the insert shows the calculated UV absorption spectra (VAMP) of a five unit oligomer of protonated pyridine moieties (Figure 3(b)).

initial viscous solution – poly(4-vinyl pyridine)/pyridine (Figure 8); and the gel (Figure 9). All optical spectra were measured on thin films placed between two quartz slides. The thickness was not controlled. The absorption spectrum of the liquid pyridine displays an absorption band at 254 nm ($\pi-\pi^*$ energy transition) with vibrational structure of the vibrational transitions 0–0, 0–1 and 0–2 (Figure 7). The absorption spectrum of the polymer dissolved in pyridine (Figure 8) has maximum intensity at 260 nm, which also is due to the $\pi-\pi^*$ energy transition. In excellent agreement with the calculated UV absorption spectrum of the oligomer, the absorption peaks of the polymer/pyridine solution are also much broader than those of the liquid pyridine (Figure 8). As expected, the absorption spectrum of the gel (Figure 9) shows an increase in intensity at 270 and 330 nm (the deconvoluted data are not shown), which in comparison with the calculated UV absorption spectrum of the oligomer with protonated species, can be assigned to an increase in the amount of self-protonated species in the gel. The extended tail in the visible range can be assigned to the long range interaction of the ordered polymer moieties in analogy to the red-shift of the same spectrum.

UV irradiation of the gel leads to a significant increase in the intensity of the absorption centred at 360 nm and to an amorphous–crystalline phase transition[12]. The photoinduced crystalline state is not stable and the material spontaneously transforms back to an amorphous gel. Calculation of the internal energy of the amorphous and crystalline phases is currently under investigation. However, the reversibility of the process shows that the crystalline phase is metastable and those photoinduced molecular retransformations are the intermediates. The reverse transition, i.e. crystalline–amorphous, are shown schematically at the molecular level in Scheme 1. The protonated quinoid structure (I), due to proton rearrangement in a ring group (II), can transform to the neutral pyridine species (III), that can maintain the gel structure via hydrogen bonding (III).

We calculate: HOMO, LUMO, dipole moment (μ) and IP of the structures I, II and III by application of the

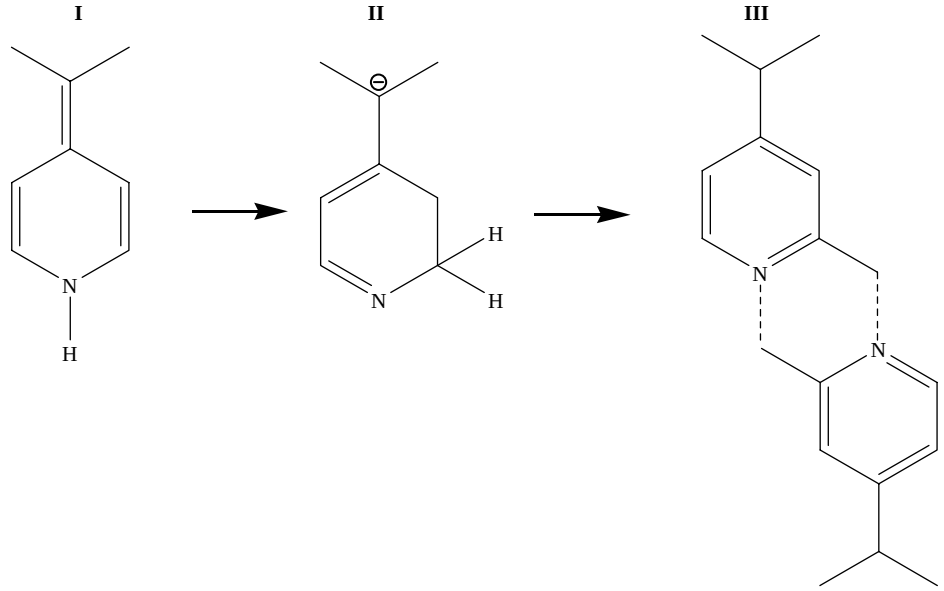

Scheme 1.

Table 2. Calculated (VAMP) HOMO, LUMO energies, ionisation potential and dipole moment for structures I, II and III (Scheme 1) and gaseous pyridine (Py).

	I	II	III	Py
HOMO (eV)	− 3.79	− 4.29	− 5.63	− 5.99
LUMO (eV)	− 1.02	− 3.50	− 1.63	− 1.94
μ (D)	2.93	3.27	0.22	2.33
IP (eV)	6.27	6.81	7.78	9.27

semiempirical program VAMP. The results are presented in Table 2, that also includes for comparison of the values for gaseous pyridine.

As can be seen, the energy of the ground state – HOMO – is significantly reduced when moving from structures I to III and approaches that of the gaseous pyridine. This reduction indicates an increase in structural stability. The energy of the lowest excited level (LUMO) is very similar in structure I and III – only the short intermediate II has a somewhat lower energy. Structure III also has the lowest value of the dipole moment (0.22 D) as well as the highest ionisation potential 7.78 eV. Thus, we can assume that the spontaneous reversion of the crystalline material to the amorphous state can be due to transformation of photoinduced protonated species to the non-protonated form.

4. Conclusion

Using the modelling programs DMol^3 and VAMP (Accelrys Inc.) we shows the effect of the self-protonation of the pyridine side-chain units on the conformational behaviour and UV absorption spectra of poly(4-vinyl pyridine). The calculated UV absorption spectra of the model compound closely reproduce the experimental data. We demonstrate that the self-protonation of the pyridine ring of poly(4-vinyl pyridine) leads to the conformational rearrangement of the pyridine ring to the quinone form as well as to rotation of the ring with respect to the alkane chain. Thus, we can suggest that this type of molecule can function in a gel as a 'working' species and is responsible for the properties of the photoinduced gel.

Acknowledgements

E.V. thanks the Israel Ministry of Absorption for financial support and Prof. N. Agmon for illuminating discussions.

References

[1] P.G. De Gennes, *Dynamics of entangled polymer solutions. I. The Rouse model*, Macromolecules 9 (1976), pp. 587–593.
[2] E. Geissler, A.-M. Hecht, C. Rochas, F. Bley, F. Livet, and M. Sutton, *Aging in a filled polymer: coherent small angle x-ray and light scattering*, Phys. Rev. E 62 (2000), pp. 8308–8313.
[3] M. Annaka and T. Tanaka, *Multiple phases of polymer gels*, Nature (1992), pp. 430–432.
[4] V.V. Vasilevskaya and A.R. Khohlov, *Swelling and collapse of polymer gel in polymer solutions and melts*, Macromolecules 25 (1992), pp. 384–390.
[5] A.V. Dobrynin and M. Rubinstein, *Theory of polyelectrolytes in solutions and at surfaces*, Prog. Polym. Sci. 30 (2005), pp. 1049–1118.
[6] A. Suzuki and T. Tanaka, *Phase transition in polymer gels induced by visible light*, Nature 346 (1990), pp. 345–347.
[7] A. Mamada, T. Tanaka, D. Kungwatchakun, and M. Irie, *Photo-induced phase transition of gels*, Macromolecules 23 (1990), pp. 1517–1519.
[8] S. Juodkazis, N. Mukai, R. Wakaki, A. Yamaguchi, S. Matsuo, and H. Misawa, *Reversible phase transitions in polymer gels induced by radiation forces*, Nature 408 (2000), pp. 178–181.
[9] T. Vikki, H. Isotalo, J. Ruokolainen, P. Passiniemi, and O. Ikkala, *Thermoreversible gels of acid doped polyaniline: electrical switching based on network transitions*, O. Synth. Met. 101 (1999), pp. 742–745.
[10] S. Champ, B. Xue, and M.B. Huglin, *Concentrating aqueous solutions of water soluble polymers by thermoreversible swelling of poly[(N-isopropylacrylamide)-co-(acrylic acid)] hydrogels*, Macromol. Chem. Phys. 201 (2000), pp. 931–940.
[11] R.A. Siegel and B.A. Firestone, *pH-dependent equilibrium swelling properties of hydrophobic polyelectrolyte copolymer gels*, Macromolecules 21 (1988), pp. 3254–3259.
[12] E. Vaganova, M. Rozenberg, and S. Yitzchaik, *Multicolor emission in poly(4-vinyl-pyridine) gel*, Chem. Mat. 12 (2000), pp. 261–263.
[13] E. Vaganova, G. Meshulam, Z. Kotler, M. Rozenberg, and S. Yitzchaik, *Photoinduced structural changes in poly(4-vinyl pyridine): a luminescence study*, J. Fluor. 10 (2000), pp. 81–88.
[14] N. Berestetsky, E. Vaganova, E. Wachtel, G. Leitus, A. Goldberg, and S. Yitzchaik, *Photoactive proton conductor: poly(4-vinyl pyridine) gel*, J. Phys. Chem. B 112 (2008), pp. 3662–3667.
[15] M. Rozenberg, E. Vaganova, and S. Yitzchaik, *FTIR study of self-protonation and gel formation in pyridinic solutions of poly(4-vinylpyridine)*, NJC 24 (2000), pp. 109–112.
[16] Accelrys, *Materials Studio Release Notes, Release 4.1*, Accelrys Software, Inc., San Diego, CA, 2006.
[17] B. Delley, *An all-electron numerical method for solving the local density functional for polyatomic molecules*, J. Chem. Phys. 92 (1990), pp. 508–517.
[18] B. Delley, *From molecules to solids with the DMol^3 approach*, J. Chem. Phys. 113 (2000), pp. 7756–7764.
[19] J.P. Perdew and Y. Wang, *Accurate and simple analytic representation of the electron-gas correlation energy*, Phys. Rev. B 45 (1992), pp. 13244–13249.
[20] J.P. Perdew and Y. Wang, *Accurate and simple density functional for the electronic exchange energy: Generalized gradient approximation*, Phys. Rev. B 33 (1986), pp. 8800–8802.
[21] J. Andzelm, R.D. King-Smith, and G Fitzgerald, *Geometry optimization of solids using delocalized internal coordinates*, Chem. Phys. Lett. 335 (2001), pp. 321–326.
[22] M.C. Zerner, G.H. Loew, R.F. Kirchner, and U.T Mueller-Westerhoff, *An Intermediate Neglect of Differential Overlap Technique for Spectroscopy of Transition-Metal Complexes. Ferrocene*, J. Am. Chem. Soc. 102 (1980), pp. 589–599.
[23] T. Clark, *A Handbook of Computational Chemistry*, Wiley, New York, 1985.